

Integrated Sideband-Resolved SERS with a Dimer on a Nanobeam Hybrid

Ilan Shlesinger,* Isabelle M. Palstra,* and A. Femius Koenderink†

Department of Physics of Information in Matter and Center for Nanophotonics,
NWO-I Institute AMOLF, Science Park 104, NL1098XG Amsterdam, The Netherlands

(Dated: August 30, 2022)

In analogy to cavity optomechanics, enhancing specific sidebands of a Raman process with narrowband optical resonators would allow for parametric amplification, entanglement of light and molecular vibrations, and reduced transduction noise. We report on the demonstration of waveguide-addressable sideband-resolved surface-enhanced Raman scattering (SERS). We realized a hybrid plasmonic-photonic resonator consisting of a 1D photonic crystal cavity decorated with a sub-20 nm gap dimer nanoantenna. Hybrid resonances in the near-IR provide designer Q-factors of 1000, and $Q/V = (\lambda^3/10^6)^{-1}$, with SERS signal strength on par with levels found in state-of-the-art purely plasmonic systems. We evidence Fano-lineshapes in the SERS enhancement of organic molecules, and quantitatively separate out the pump-enhancement and LDOS contributions.

Molecules can exchange energy with incident light through the vibrations of their atomic bonds [1]. The resulting inelastic light scattering, called Raman scattering, is routinely used for molecular detection or material characterization and underlies applications like Raman amplifiers and lasers. Surface-enhanced Raman spectroscopy (SERS) uses plasmonic nanoparticles featuring intense field hotspots to enhance the intrinsically weak Raman scattering of molecules by orders of magnitude, and is among the most popular tools to reach single molecule sensitivities [2–5]. Recently, theoretical efforts have sought to exploit formal analogies between SERS and cavity optomechanics [6–10], which is the field of precisely controlling and sensing the motion of mechanical resonator modes through radiation pressure in suitably tailored optical cavities. This field has witnessed breakthroughs such as parametric cooling and amplification of motion, strong optomechanical coupling, measurement of motion near the quantum limit, optomechanical entanglement, frequency conversion, and production of non-classical mechanical states [11, 12]. The molecular optomechanics viewpoint promises to bring these exciting effects that were obtained in nano-engineered MHz/GHz acoustic resonators to terahertz and mid-IR molecular vibrations, with already demonstrations of coherent wavelength conversion [13, 14], and possibly the study of non-classical correlations with molecules [15, 16].

A central tenet of cavity optomechanics is that so-called sideband-resolved operation is crucial, which is attained when the optical cavity has a linewidth smaller than the mechanical resonance frequency [11, 12]. It eliminates detrimental backaction, thus allowing ground-state cooling, pure light-mechanical entanglement, and frequency conversion without added noise. Generally, by selecting pure Stokes or anti-Stokes transitions, pure beam-splitter or two-mode squeezing interactions are generated between optical and mechanical degrees of freedom. High-quality factor dielectric cavities can provide the narrowband spectral structure required for sideband-resolved SERS, but are limited to low electric field con-

finement. Such systems result in very low Raman enhancement and small optomechanical coupling strengths and are orders of magnitude away from SERS enhancement factors competitive with plasmonic systems. Conversely, the optical linewidth ($Q=10\text{--}30$) for typical plasmon antennas [17] exceeds the vibrational frequencies, so that established SERS geometries are not sideband-resolved. A major challenge is how to reach sideband resolution while maintaining the uniquely strong field enhancement of metal junctions. Furthermore, a main open question for both traditional SERS and prospective molecular-sideband resolved optomechanics is how to achieve waveguide-addressability. All SERS demonstrations with few molecules have been limited to free-space configurations, since integrated geometries are rapidly confronted to high background noise emanating from the guiding material [18, 19].

In this Letter, we report on the realization of a proposed new generation of hybrid light resonators [20–22] that combine a plasmonic antenna interacting with a dielectric cavity and features narrow and intense resonances [23–25]. We show how it allows for few-molecules sideband-resolved SERS with selective enhancement of single Raman lines and with waveguide excitation / collection capabilities (Fig. 1(a)). The system combines photonic crystal nanobeam cavities [26] with single gold dimer antennas [27], aligned to within a few nanometers (Fig. 2(B)) by two-step lithography. Due to the complexity of positioning two optical resonators relative to each other with high accuracy, so far only hybrid resonators with simple geometries featuring the simplest antennas have been demonstrated, lacking the field confinement required for SERS [28]. We overcome this limitation and combine a precisely aligned gap-antenna geometry, with tightly confined dielectric microcavities. The plasmonic-photonic hybridization creates sharp features in the optical reservoir [29], i.e., in the local density of optical states (LDOS) landscape felt by the Raman species with which we functionalized the gold antennas. We present a study using a confocal Raman spectroscopy setup (Fig. 1(b))

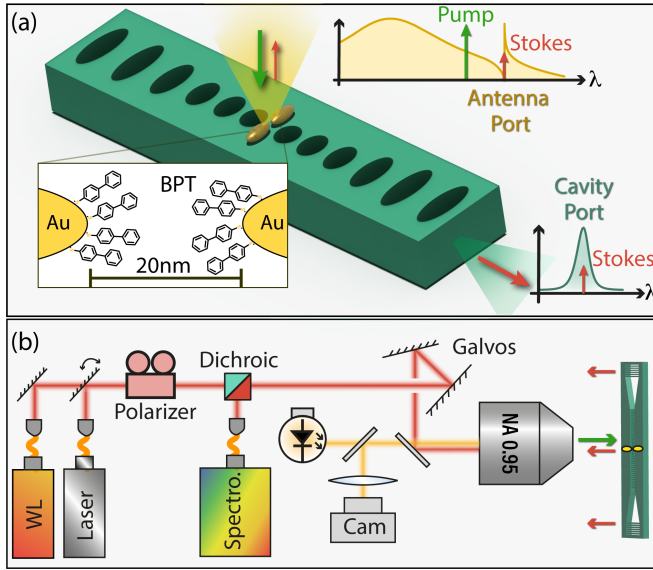


FIG. 1. (a) Sketch of a gold dimer hybridizing with a Si_3N_4 photonic crystal nanobeam cavity. The resulting narrow linewidth and intense optical mode couples to BPT molecules self-assembled on the antenna surface. Specific Raman sidebands can be selectively enhanced and addressed both in free-space or in a waveguide. Depending on the addressed optical port, the enhancement will feature a Fano lineshape or Lorentzian-like shape. (b) Confocal Raman microscope with a tunable laser to scan over the hybrid resonances.

with a tunable Raman pump laser, disentangling the role of pump enhancements and the LDOS landscape, and evidencing waveguide-addressed sideband-resolved SERS.

SEM micrographs in Fig. 2(a,b) show a representative example of a hybrid, composed of a gold dimer antenna placed on top and in the center of a Si_3N_4 photonic crystal [26, 28]. The beams lie on $8 \mu\text{m}$ of SiO_2 to optically separate them from the Si substrate, and are designed for resonance wavelengths near 780 nm. The nanobeam cavity is designed with two gratings on each side to couple light in and out from free-space to the waveguide. The antennas are gold ellipsoids of 20 nm short axis and variable long axis (50 to 80 nm) and feature strong field confinement in the 20 nm gap. While the aligned multi-step electron-beam lithography required to realize these samples is challenging, the robustness of our fabrication protocol is evident from the fact that our study is based on optical measurements on over 280 of such hybrid resonators, where we systematically sweep the cavity and antenna resonance by sweeping their geometry (in-plane size parameter). [30]. Design quality factors predict $Q_c \simeq 2500$ and mode volumes $V_c \sim 3\lambda^3$ for the nanobeam and $V_a = 10^{-4}\lambda^3$ for the dimers, resulting in $Q \sim 10^3$ and $V \sim 2 \times 10^{-3}\lambda^3$ for hybrids [21]. The resulting Q/V ratio of 10^6 in units of λ^3 is on par with state-of-the-art nanoparticle-on-mirror constructs in plasmonics [31] on one hand, and with photonic crystal cavities [26] on the

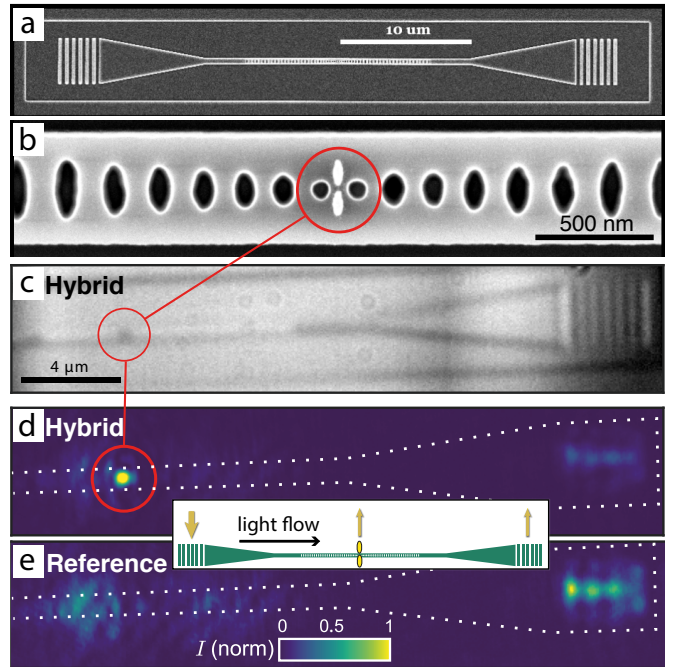


FIG. 2. (a) SEM micrograph of a nanobeam cavity with grating couplers on each side. (b) Aligned dimer antenna placed on top and in the center of the cavity. (c) Bright-field WL microscopy image showing the cavity (left-hand part of figure) and grating outcoupler (right-hand). The antenna appears as a black dot. (d-e) Laser scattering of the same device (d and c) and a device with no antenna (e). The system is driven by a laser resonant with the cavity, and focused on the left incoupling grating (not visible here). Bright scattering by the antenna demonstrates antenna-cavity coupling.

other, but with the unique asset that Q can be chosen at will from 10^2 to 10^3 .

Fig. 3(a,b) reports on the measured resonance properties of the individual constituents, that is, antenna and cavity. Antenna darkfield (DF) spectra (Fig. 3(a)) confirm that the dimer antennas feature a dipolar resonance polarized along the long axis of the antennas and that can be tuned with the long-axis length. Quality factors around 10 are extracted by fitting the spectra with squared Lorentzians [32]. We quantify the cavity resonances by waveguide transmission spectra, focusing light from a fiber-coupled white-light (WL) halogen lamp on one grating coupler and collecting from the other. Fig. 3(b) shows spectra of antenna-free nanobeams. The resonance wavelength can be tuned by the position and width of the holes, with a tuning range from 772 to 800 nm obtained for a 4% size difference (Fig. 3(c), full dots). As shown in Fig. 3(d), the bare cavity modes have measured $Q \sim 600$ with strong variability due to fabrication imperfections, and with the highest values obtained equal to $Q \simeq 1000$.

With regard to hybrid cavity-antenna structures, the first signatures of hybridization are readily observed

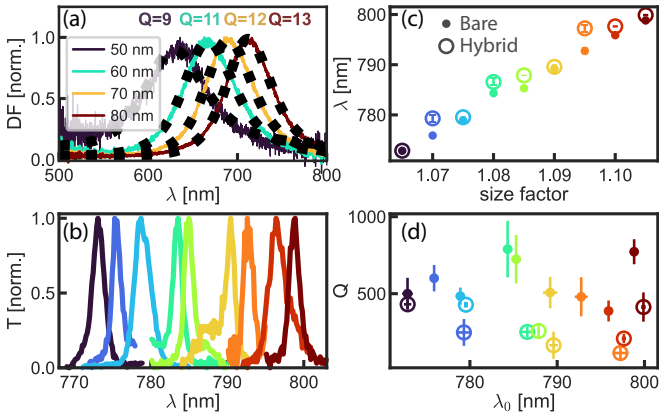


FIG. 3. (a) DF spectra of bare gold dimers. Resonances redshift with antenna size. Q's are extracted from squared Lorentzian fits (dotted lines). (b) Transmission of bare nanobeam cavities. Increasing the in-plane photonic crystal hole radius and period (scaling parameter on x -axis) tunes the cavity resonance (c). In the presence of the antenna, the hybridized cavity mode is red-shifted and broadened (open circular markers) (c-d). Errorbars are standard deviations from four different but nominally identical beams/hybrids.

in the spatial scattering of the cavity presented in Fig. 2(d,e). For Fig. 2(d,e), the beam from a tunable diode laser (Toptica DL-pro) is aimed at the incoupling grating located on the left-hand side of the image, just outside the field of view. For both the hybrid and the reference (panel d versus e), scattering emanates from both the cavity region, and the output grating only when the laser is tuned to resonance with the cavity (ca. 780 nm). For the hybrid system, there is bright scattering from the antenna (bright dot in (d); the antenna appears as a dark spot in bright-field microscopy (c)). On the contrary, in absence of an antenna, the light is mainly outcoupled from the second grating (Fig. 2(e)), and the cavity area itself only shows dim and spatially distributed scattering. This shows that it is possible to drive the gold dimer antenna through the nanobeam structure, implying optical coupling between the cavity mode and the plasmon antenna resonance. As shown below, this coupling provides frequency structure in hybrid LDOS enhancement and waveguide addressability of the plasmonic hot spot.

To further characterize the hybridization of microcavity and antenna, we turn back to the WL transmission spectra. Figs. 3(c,d) present extracted resonance wavelengths λ_0 and Q for many hybrid devices with circled markers, to be directly compared with the bare nanobeam data (closed symbols). Although the scatter in the nanobeam λ_0 and Q due to nanometer fabrication fluctuations makes it difficult to directly measure cavity perturbation effects by comparing different devices, we find that hybridized resonances appear systematically redshifted and broadened compared to bare cavities, as expected from cavity perturbation theory [33], with a re-

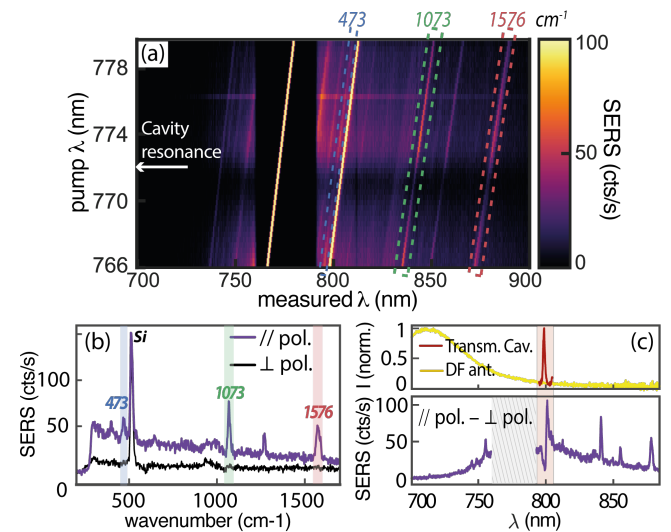


FIG. 4. (a) SERS on a hybrid for pump wavelengths scanned from 766 to 780 nm. The Fano response of the hybridized antenna can be seen as a lowering and raising of SERS intensity when passing through the cavity resonance frequency (pump enhancement effect, near 772 nm). (b) Cross-cut of (a) for $\lambda_{\text{pump}} = 774$ nm (purple line). Raman scattering from the BPT is only detected when the laser is polarized parallel to the dimer. For orthogonal polarization, only the Si signal from the substrate is seen (black curve). (c) Darkfield and transmission spectrum of a hybrid where the cavity resonance at 800 nm lies in the Stokes sideband (LDOS enhancement). Bottom: SERS spectrum featuring a clear Fano resonance (silicon background subtracted).

duction in quality factor towards the Q=200-300 range (Fig. 3(c,d), circles). These Q are ideally suited for sideband-resolved SERS. At our operation wavelength, Q=200 corresponds to ca. 65 cm^{-1} : sufficiently narrow to select single low frequency vibrational lines, yet wide enough to encompass typical Raman linewidths in full [1].

In the following, the waveguide-addressable hybrid plasmonic-photonic mode is used to explore sideband-resolved SERS. To this end we functionalize the gold antennas with biphenyl-4-thiol (BPT) molecules which form self-assembled monolayers on gold, and exhibit distinct Raman scattering [34]. After functionalization, the system is encapsulated in PMMA to provide the host index required for the nanobeam mode. Fig. 4(a) shows a set of Raman spectra recorded on a hybrid as function of both detection wavelength and pump wavelength. As the pump laser is swept from 766 to 780 nm (residual transmitted pump light through the notch filter weakly visible), the BPT Raman lines (lines of interest highlighted in dashed boxes) maintain a constant shift from the laser frequency. In Fig. 4(a) the cavity resonance lies at 772 nm, and the hybrid Fano response of the antenna at the cavity frequency results in a Fano shaped pump enhancement while scanning the laser, reducing the pump field enhancement at the Fano dip around 771 nm and

increasing it at the Fano peak around 774 nm. The intensity of the electronic Raman scattering [35] (broad Raman background) and the narrow BPT Raman peaks show this trend in the pump enhancement most noticeably as the clear dark region around 771 nm in Fig.4(a). Instead, the silicon peak (bright line at 520 cm^{-1}) emitted by the underlying substrate has a constant intensity, evidencing that the signal modulation is actually due to the hybrid resonance and not to an overall change in pump laser intensity. To further check that the SERS signal comes strictly from BPT molecules at the antenna, we plot in Fig. 4(b) a cross-cut of the Raman spectrum recorded at $\lambda_{\text{laser}} = 774 \text{ nm}$ for a laser polarization parallel to the dimer long axis (full line) and a reference case with pump polarization along the short axis. SERS signal is observed only for the parallel case, whereas no BPT Raman peaks appear in the orthogonal configuration, and only the Raman line from the underlying silicon substrate is observed (520 cm^{-1}). The intermediate glass and PMMA cladding do not contribute to the Raman signal. Considering that the BPT counts in the reference case are below noise levels of 1 count/s we deduce a lower bound on Raman enhancement of 1.1×10^4 , limited by our ca. 20 min. integration time, although the actual enhancement is expected to be 2-3 orders of magnitude larger [30].

To highlight the effect of hybrid LDOS, Fig. 4(c) shows a Raman spectrum from a hybrid with $\lambda_0 = 800 \text{ nm}$ that now lies in the Stokes sideband (Fig. 4(c)). For reference, the diagram shows the relevant antenna dark-field spectrum and cavity transmission. Interference of the narrow-cavity resonance and the broad dimer response results in a structured LDOS with a Fano lineshape. This Fano resonance is imprinted on the broad Raman background, attributed to electronic Raman scattering of the gold, around 800 nm wavelength (bottom panel). For this example, we tuned the Fano peak to enhance the BPT line at 473 cm^{-1} . Combined, Figs. 4(a) and (c) qualitatively show that it is possible to superimpose the hybrid resonance selectively with either the pump wavelength or with specific Raman lines.

To quantitatively analyze the effect of the hybrid mode on SERS through pump and LDOS enhancement, Fig. 5 compares in more detail the two different cases where the hybrid mode is either resonant with the laser pump or is instead red-shifted to overlap selectively with one of the BPT peaks. We first discuss the SERS response of hybrids tuned to resonance with the pump wavelength, as reported in the left columns of Fig. 5 (panels a1–c1). Panel (a1) reports WL transmission, evidencing a hybrid resonance at $\lambda_0 = 772 \text{ nm}$ and $Q = 323$. Panels b1 and c1 are excitation spectra reporting integrated counts in the Raman lines at 473 , 1073 , and 1576 cm^{-1} (blue, green and red curves) as function of pump wavelength (swept from 765 – 780 nm at $400 \mu\text{W}$ power, 20 s integration time per data point). Fig. 5(b1) is for free space

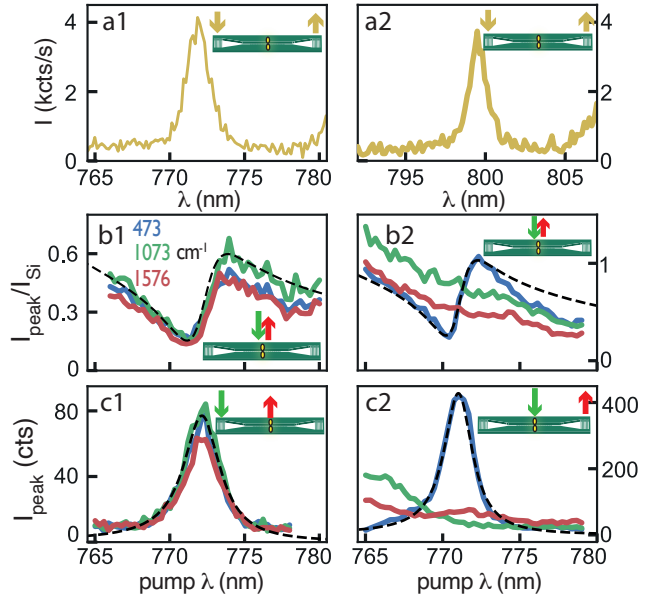


FIG. 5. Pump (left column) or LDOS (right column) hybrid enhancement and selective collection in the waveguide. (a) WL transmission spectrum of the hybridized cavity resonance. (b,c) Integrated counts of 3 selected BPT Raman peaks intensities for laser wavelengths from 765 to 780 nm. In (b) pump and collection is through the antenna and normalized by the Si line, taken as reference. (c1) coupling through one grating and collecting at the antenna and (c2) is the inversed configuration. Dashed curves are from a semi-analytical theoretical model [30].

excitation directly focused on the antenna, and signal collection from the same location and through the same objective. To compensate for minor differences in incoupled laser power the signals are normalized by the 520 cm^{-1} Si Raman line from the underlying substrate, which is unperturbed by the hybrid. A clear Fano lineshape is observed for the integrated counts of each peak as the laser is tuned over the hybrid resonance. All three Raman lines follow the same Fano line-shape, consistent with the expectation that the SERS enhancement is the product of a pump-field enhancement factor (resonator property at the pump frequency) and LDOS enhancement at the Stokes-shifted frequency. In this scenario the pump enhancement that is common to all three lines shows the hybrid Fano-lineshape, while the LDOS at the Stokes-shifted frequencies is unstructured. Indeed, since the Stokes lines are all detuned well away from the cavity, their LDOS is essentially in the featureless wing of the broad Lorentzian antenna resonance. The Fano lineshape in the pump enhancement occurs because free-space pumping directly drives the broad antenna resonance, and its coupling to the narrow resonance appears as a transparency line [25, 36]. Panel (c1) shows SERS results on the same hybrid, but interrogated through a different input channel as excitation is now through the

waveguide and cavity. To this end, we align the pump laser to one of the gratings, but still collect light from the antenna location. We obtain a clear BPT Raman signal. When we sweep the laser frequency, all three Raman lines again follow a very similar behavior. However, instead of a Fano lineshape, the SERS enhancement now traces an almost Lorentzian resonance. This observation can again be rationalized from the fact that SERS enhancement is due to a strong spectral modification of the pump enhancement, yet an unstructured LDOS at the vibrational lines. The Lorentzian line reports the transfer function for pump light from the grating coupler, via the cavity, to the antenna.

We now turn to the second scenario, wherein the hybrid provides selective LDOS enhancement, instead of pump enhancement. To this end, we select a different cavity with a longer resonance wavelength at 800 nm with $Q \sim 640$ as established by the transmission spectrum in Fig. 5(a2). In contrast to the previous scenario, now the pump laser is not tuned through the hybrid resonance but through a wavelength interval blue-detuned by about 25 nm, exactly such that a single Stokes-shifted Raman peak tunes across the hybrid resonance (same structure as in Fig. 4(c)). The results are shown in the right column of Fig. 5. When the laser wavelength is swept from 765 nm to 779 nm, only the BPT Raman line at 473 cm^{-1} is scanned across the hybrid resonance. The structure is again first interrogated by free-space pumping and collection on / from the antenna. In stark contrast to the earlier results now just one Raman line shows a Fano lineshape, while the other Raman lines follow a broad shoulder. This is consistent with the notion that the pump field now enjoys the broadband enhancement of the antenna, without modification by the cavity mode, and that the hybrid LDOS shows a Fano line that acts only on the vibration that it is resonant with (here the 473 cm^{-1} line). The shoulder in the other lines is due to the typical SERS enhancement of the bare antenna, which decreases as one tunes away from resonance [37].

Finally, Fig. 5(c2) shows waveguide addressed SERS. As the photonic crystal cavity prohibits optical transport between the grating coupler and antenna except on cavity resonance, the pump light is now provided from free space, while the Raman signal is collected from the outcoupling grating. Only when aligning the 473 cm^{-1} Stokes-shifted line to the hybrid resonance, one would expect Raman scattered light to be transmitted through the photonic crystal nanobeam cavity and collected at the grating. Indeed, the 1073 and 1576 cm^{-1} Raman lines barely pass through the waveguide, whereas the 473 cm^{-1} line shows a strong Lorentzian resonance. Here, the pump enhancement still originates from the broad antenna resonance, while the hybrid resonance provides both the LDOS and the collection efficiency into the waveguide required to enhance and efficiently collect only a single Raman line. Importantly, the SERS enhance-

ment for integrated operation is as good as into free space (see [30] for further analysis of signal levels). Indeed, the cavity parameters ensure a good trade-off between hybrid enhancement and collection rates [21, 25].

To conclude, we reported on the realization of a new generation of hybrid plasmonic-dielectric cavity resonators, with a lithographically designed gap antenna accurately coupled to a narrow linewidth photonic crystal cavity. The hybrid resonances allow one to selectively enhance and collect single Raman lines in a guided mode, paving the way for on-chip applications of spectrometer-free, specific Raman species detection. The intense resonances obtained with the 20 nm gap modes, and the narrow linewidth obtained through hybridization with the high-Q cavity mode are particularly interesting for sideband-resolved molecular optomechanics. For instance, sideband resolution is highly relevant to observe parametric instabilities in the few molecule regime [9]. Achieving this regime would require further optimization of cavity fabrication to reach higher quality factors as expected for photonic crystal geometries [38]. Indeed, we estimate the optomechanical cooperativity C_m , which determines the degree of coherence of the light-vibration interaction, to be on the order of 10^{-3} for our system. Cooperativities $C_m \gtrsim 1$ are expected for challenging, yet realistically achievable parameters $Q_c \simeq 5000$ and dimer gaps of 4 nm.

ACKNOWLEDGEMENTS

We thank Alejandro Martínez and Ewold Verhagen for stimulating discussions. This work is part of the Research Program of the Netherlands Organization for Scientific Research (NWO). The authors acknowledge support from the European Unions Horizon 2020 research and innovation program under Grant Agreements No. 829067 (FET Open THOR).

* Equal contribution

† f.koenderink@amolf.nl

- [1] D. A. Long, *The Raman effect: a unified treatment of the theory of Raman scattering by molecules* (Wiley, Chichester ; New York, 2002).
- [2] M. Fleischmann, P. Hendra, and A. McQuillan, Raman spectra of pyridine adsorbed at a silver electrode, *Chem. Phys. Lett.* **26**, 163 (1974).
- [3] D. L. Jeanmaire and R. P. Van Duyne, Surface Raman spectroelectrochemistry: Part i. heterocyclic, aromatic, and aliphatic amines adsorbed on the anodized silver electrode, *J. Electroanal. Chem. Interfacial Electrochem.* **84**, 1 (1977).
- [4] M. G. Albrecht and J. A. Creighton, Anomalously intense Raman spectra of pyridine at a silver electrode, *J. Am. Chem. Soc.* **99**, 5215 (1977).

[5] E. C. Le Ru and P. G. Etchegoin, Single-molecule surface-enhanced Raman spectroscopy, *Annu. Rev. Phys. Chem.* **63**, 65 (2012).

[6] P. Roelli, C. Galland, N. Piro, and T. J. Kippenberg, Molecular cavity optomechanics as a theory of plasmon-enhanced Raman scattering, *Nat. Nanotechnol.* **11**, 164 (2016).

[7] M. K. Schmidt, R. Esteban, A. González-Tudela, G. Giedke, and J. Aizpurua, Quantum mechanical description of Raman scattering from molecules in plasmonic cavities, *ACS Nano* **10**, 6291 (2016).

[8] F. Benz, M. K. Schmidt, A. Dreismann, R. Chikkaraddy, Y. Zhang, A. Demetriadou, C. Carnegie, H. Ohadi, B. De Nijs, R. Esteban, J. Aizpurua, and J. J. Baumberg, Single-molecule optomechanics in "picocavities", *Science* **354**, 726 (2016).

[9] A. Lombardi, M. K. Schmidt, L. Weller, W. M. Deacon, F. Benz, B. de Nijs, J. Aizpurua, and J. J. Baumberg, Pulsed molecular optomechanics in plasmonic nanocavities: from nonlinear vibrational instabilities to bond-breaking, *Phys. Rev. X* **8**, 011016 (2018).

[10] M. K. Schmidt, R. Esteban, F. Benz, J. J. Baumberg, and J. Aizpurua, Linking classical and molecular optomechanics descriptions of SERS, *Faraday Discuss.* **205**, 31 (2017).

[11] M. Aspelmeyer, T. J. Kippenberg, and F. Marquardt, Cavity optomechanics, *Rev. Mod. Phys.* **86**, 1391 (2014).

[12] W. P. Bowen, G. J. Milburn, and G. J. Milburn, *Quantum optomechanics* (CRC Press, 2015).

[13] W. Chen, P. Roelli, H. Hu, S. Verlekar, S. P. Amirtharaj, A. I. Barreda, T. J. Kippenberg, M. Kovylina, E. Verhagen, A. Martínez, and C. Galland, Continuous-wave frequency upconversion with a molecular optomechanical nanocavity, *Science* **374**, 1264 (2021).

[14] A. Xomalis, X. Zheng, R. Chikkaraddy, Z. Koczor-Benda, E. Miele, E. Rosta, G. A. E. Vandenbosch, A. Martínez, and J. J. Baumberg, Detecting mid-infrared light by molecular frequency upconversion in dual-wavelength nanoantennas, *Science* **374**, 1268 (2021).

[15] Y. Zhang, J. Aizpurua, and R. Esteban, Optomechanical collective effects in surface-enhanced Raman scattering from many molecules, *ACS Photonics* **7**, 1676 (2020).

[16] V. Vento, S. T. Velez, A. Pogrebna, and C. Galland, Measurement-Induced Collective Vibrational Quantum Coherence under Spontaneous Raman Scattering in a Liquid (2022), arXiv:2105.00213 [physics, physics:quant-ph].

[17] M. Agio and A. Alù, *Optical antennas* (Cambridge University Press, 2013).

[18] F. Peyskens, A. Dhakal, P. Van Dorpe, N. Le Thomas, and R. Baets, Surface enhanced Raman spectroscopy using a single mode nanophotonic-plasmonic platform, *ACS Photonics* **3**, 102 (2016).

[19] F. Peyskens, P. Wuytens, A. Raza, P. V. Dorpe, and R. Baets, Waveguide excitation and collection of surface-enhanced raman scattering from a single plasmonic antenna, *Nanophotonics* **7**, 1299 (2018).

[20] Y.-F. Xiao, Y.-C. Liu, B.-B. Li, Y.-L. Chen, Y. Li, and Q. Gong, Strongly enhanced light-matter interaction in a hybrid photonic-plasmonic resonator, *Phys. Rev. A* **85**, 031805 (2012).

[21] H. M. Doeleman, E. Verhagen, and A. F. Koenderink, Antenna-cavity hybrids: matching polar opposites for Purcell enhancements at any linewidth, *ACS Photonics* **3**, 1943 (2016).

[22] K. D. Heylman, N. Thakkar, E. H. Horak, S. C. Quillin, C. Cherqui, K. A. Knapper, D. J. Masiello, and R. H. Goldsmith, Optical microresonators as single-particle absorption spectrometers, *Nat. Photonics* **10**, 788 (2016).

[23] M. K. Dezfouli and S. Hughes, Quantum optics model of surface-enhanced Raman spectroscopy for arbitrarily shaped plasmonic resonators, *ACS Photonics* **4**, 1045 (2017).

[24] M. K. Dezfouli, R. Gordon, and S. Hughes, Molecular optomechanics in the anharmonic cavity-QED regime using hybrid metal-dielectric cavity modes, *ACS Photonics* **6**, 1400 (2019).

[25] I. Shlesinger, K. G. Cognée, E. Verhagen, and A. F. Koenderink, Integrated molecular optomechanics with hybrid dielectric–metallic resonators, *ACS Photonics* **8**, 3506 (2021).

[26] P. B. Deotare, M. W. McCutcheon, I. W. Frank, M. Khan, and M. Lončar, High quality factor photonic crystal nanobeam cavities, *Appl. Phys. Lett.* **94**, 121106 (2009).

[27] P. J. Schuck, D. P. Fromm, A. Sundaramurthy, G. S. Kino, and W. E. Moerner, Improving the mismatch between light and nanoscale objects with gold bowtie nanoantennas, *Phys. Rev. Lett.* **94**, 017402 (2005).

[28] I. M. Palstra, H. M. Doeleman, and A. F. Koenderink, Hybrid cavity-antenna systems for quantum optics outside the cryostat?, *Nanophotonics* **8**, 1513 (2019).

[29] M. Kamandar Dezfouli, R. Gordon, and S. Hughes, Modal theory of modified spontaneous emission of a quantum emitter in a hybrid plasmonic photonic-crystal cavity system, *Phys. Rev. A* **95**, 013846 (2017).

[30] See Supplemental Material at [URL will be inserted by publisher] for fabrication and experimental details, mode simulations versus geometry, and semi-analytical line-shape modelling.

[31] J. J. Baumberg, J. Aizpurua, M. H. Mikkelsen, and D. R. Smith, Extreme nanophotonics from ultrathin metallic gaps, *Nature Materials* **18**, 668 (2019).

[32] C. F. Bohren and D. R. Huffman, *Absorption and scattering of light by small particles*, 1st ed. (Wiley, 1998).

[33] H. Bethe and J. Schwinger, *Perturbation Theory for Cavities* (Massachusetts Institute of Technology, Radiation Laboratory, Cambridge, MA, 1943).

[34] C. D. Bain, H. A. Biebuyck, and G. M. Whitesides, Comparison of self-assembled monolayers on gold: coadsorption of thiols and disulfides, *Langmuir* **5**, 723 (1989).

[35] J. Mertens, M.-E. Kleemann, R. Chikkaraddy, P. Narang, and J. J. Baumberg, How light is emitted by plasmonic metals, *Nano Lett.* **17**, 2568 (2017).

[36] F. Pan, K. C. Smith, H. L. Nguyen, K. A. Knapper, D. J. Masiello, and R. H. Goldsmith, Elucidating energy pathways through simultaneous measurement of absorption and transmission in a coupled plasmonic–photonic cavity, *Nano Lett.* **20**, 50 (2020).

[37] A. D. McFarland, M. A. Young, J. A. Dieringer, and R. P. Van Duyne, Wavelength-scanned surface-enhanced Raman excitation spectroscopy, *J. Phys. Chem. B* **109**, 11279 (2005).

[38] Q. Quan and M. Lončar, Deterministic design of wavelength scale, ultra-high Q photonic crystal nanobeam cavities, *Opt. Express* **19**, 18529 (2011).

Supplementary Information - Integrated Sideband-Resolved SERS with a Dimer on a Nanobeam Hybrid

Ilan Shlesinger,* Isabelle M. Palstra,* and A. Femius Koenderink[†]

*Department of Physics of Information in Matter and Center for Nanophotonics,
NWO-I Institute AMOLF, Science Park 104,
NL1098XG Amsterdam, The Netherlands*

(Dated: August 30, 2022)

Fabrication - A two-step lithography process allows to fabricate the dimer exactly on top of the center of a photonic crystal cavity. The full procedure is sketched in Fig. 1.(a-c) The cavity is fabricated by etching a photonic crystal into Si_3N_4 on a glass substrate. (d-h) A subsequent lithography step using a Ge hard mask allows fabricating a dimer antenna with a small ~ 20 nm gap on top of the photonic crystal cavity. Markers created in the first step that allow for the precise alignment of the dimer and the cavity center for proper hybridization of the two optical modes.

Optical setup - The measurements are performed on a home-built confocal Raman spectroscopy setup. The signal is collected with a microscope objective (Olympus MPlan IR, 100X, NA= 0.95) and routed to a fiber-coupled spectrometer (Andor Shamrock A-SR-303i-B-SIL) equipped with a cooled silicon CCD camera (Andor iVac A-DR324B-FI). Excitation is performed with a narrowband tunable diode laser (Toptica DL-Pro 780), spectrally cleaned with a pair of bandpass filters (Semrock TBp01-790/12). Prior to insertion of detected light into the collection fiber, Rayleigh scattered light is filtered with a set of two notch filters (Thorlabs NF785-33). This configuration allows for the detection of both Stokes and anti-Stokes signals, with the pump frequency being tuned over a relevant range (tens of

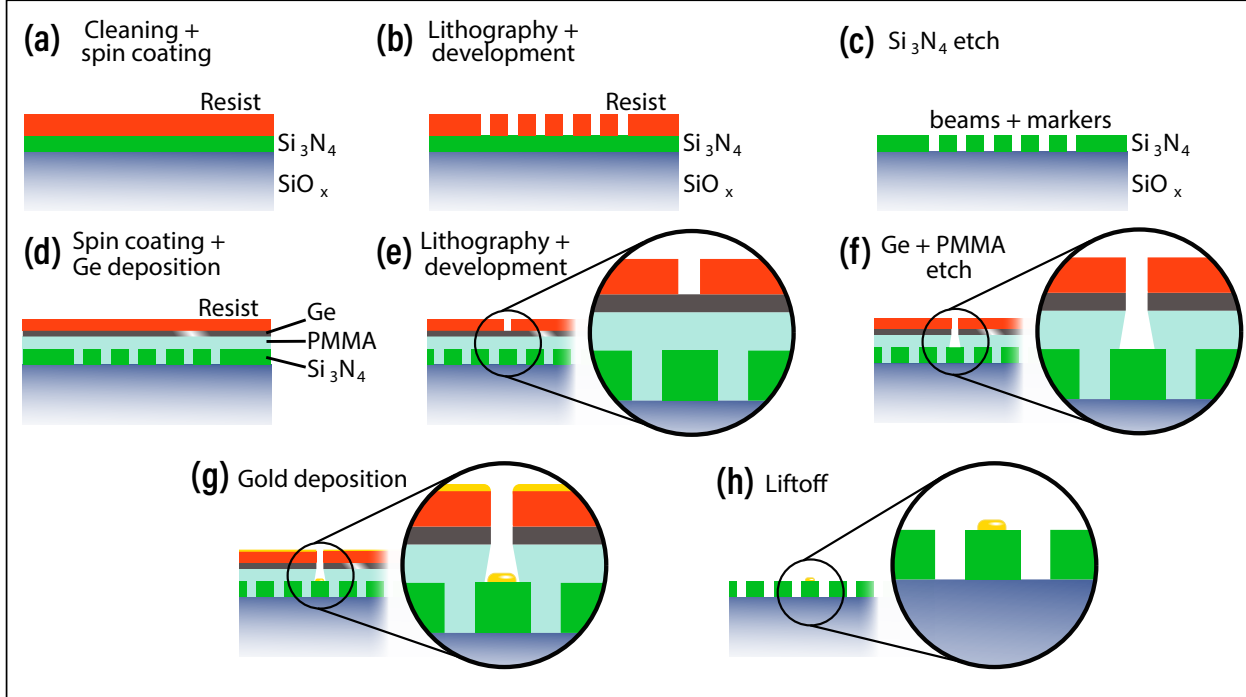


FIG. 1. Fabrication steps of the dimer on nanobeam hybrid.

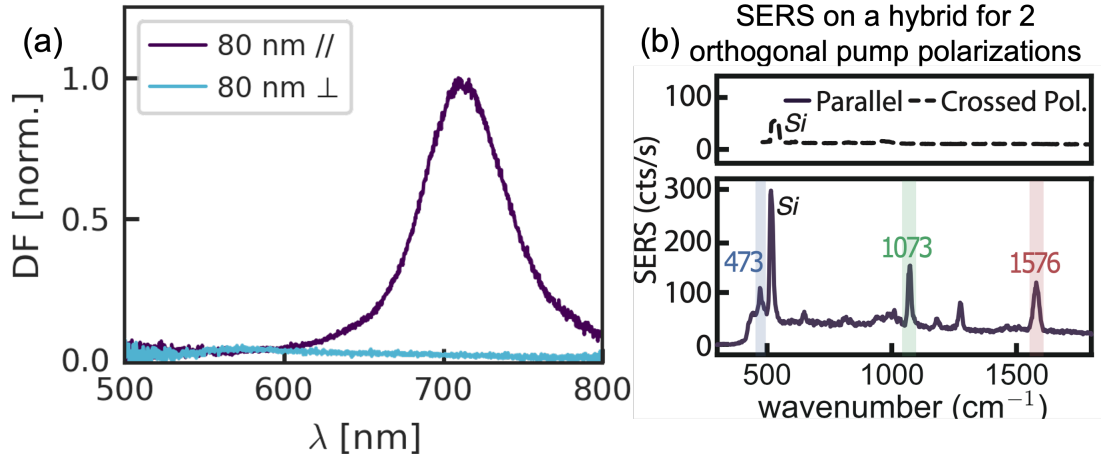


FIG. 2. (a) Two DF spectra for incident light polarized parallel or orthogonal to the long axis of the dimers. The sample is a field of dimer antennas on glass at a distance of 2 μm from each other, covered with PMMA. Measurements are performed with a Nikon LV-UEPI2 epi illumination unit, using a 100 W halogen light source and a Nikon 20X, NA0.45, DF objective. The collected light is injected into a 200 μm optical fiber connected to a spectrometer (Avantes 2048TEC-2-USB2, fan-cooled CCD). Approximately 20 antennas lie on the collection spot. (b) SERS spectrum for orthogonal (top) and parallel (bottom) polarization of the laser pump w.r.t. the dimer long axis. The reference case was obtained after 20 min integration time, resulting in a saturation of the CCD for the main Si Raman peak (520 cm^{-1}).

nanometers).

Lower bound on Raman enhancement - A lower bound on the Raman enhancement of the hybrid can be obtained by comparing the counts obtained when the hybrid is excited with those of a reference case. The anisotropy of the dimer antenna results in a very different resonance frequency for the plasmonic mode depending on the polarization of the electric field, and only a beam polarized along the long axis of the dimers can excite the dimer resonance as shown in the DF spectra of Fig. 2. A reference case for each hybrid resonator is then obtained by simply turning the polarization of the excitation laser so as to be orthogonal to the long axis of the dimer. A measurement with a 20 minute integration time (limited by small mechanical drifts at larger time scales) is shown in Fig. 2(b). Only the Raman peaks from the silicon (the 520 cm^{-1} saturating the CCD) are visible, with no signal from the BPT (lower than the noise background of about 1ct/s). Compared to the BPT

signal obtained from the same sample when the dimer is excited with a parallel polarization, we deduce a minimum SERS enhancement of the hybrid of the order of 1.1×10^4 . Using a semi-analytical model, we expect this value to be much lower than the actual enhancement, which we predict to be on the order of 10^{6-7} (see below).

Simulation - The SERS enhancement of the hybrid with two optical modes and different input and output ports can be compared to a semi-analytical model presented elsewhere [1]. This model is based on semi-classical Langevin equations describing multiple optical modes with different input and output ports, coupled to a mechanical resonance. The model is fitted to the experimental data, with initial values obtained from finite-element COMSOL simulations. Importantly, both direct (antenna in, antenna out) and crossed configurations (with input or output through the waveguide) are simultaneously fitted with the same parameters for each hybrid. The Stokes enhancement for the two hybrids studied in the main text are shown in Fig. 3 (for a single input-output port configuration for each hybrid as an example). The Stokes enhancement predicted by the model is on the order of 10^{6-7} and is almost equal for a collection through the antenna or a collection in the waveguide. The final values of the parameters for the pump-enhancement hybrid are summarized in table I. Most

Parameters	Cavity	Antenna	Comment
Frequency [THz]	389	425	From WL and DF, fitted
Q	380	10	WL and DF, fit for cavity
Mode Volume (in λ^3)	12	10^{-4}	COMSOL, fitted for the cavity
Ohmic losses γ_i [$2\pi \times \text{THz}$]	-	19.9	COMSOL
Radiative losses γ_{rad} [$2\pi \times \text{THz}$]	-	23	DF
Incoupling efficiency η_{in}	0.022	0.24	NA=0.9, see text
Outcoupling efficiency η_{out}	0.13	0.24	idem

TABLE I. Simulation parameters for the beam with a cavity resonant to the pump. Similar values are obtained for the beam with a hybrid enhancement of the LDOS. The source of the parameter value is given in the last column. When fitted, the parameters are constrained to values close to initial values obtained from FEM simulation.

of the parameters can be estimated from WL measurements and FEM calculations. Only remaining are the input and output coupling efficiencies. The input and output coupling

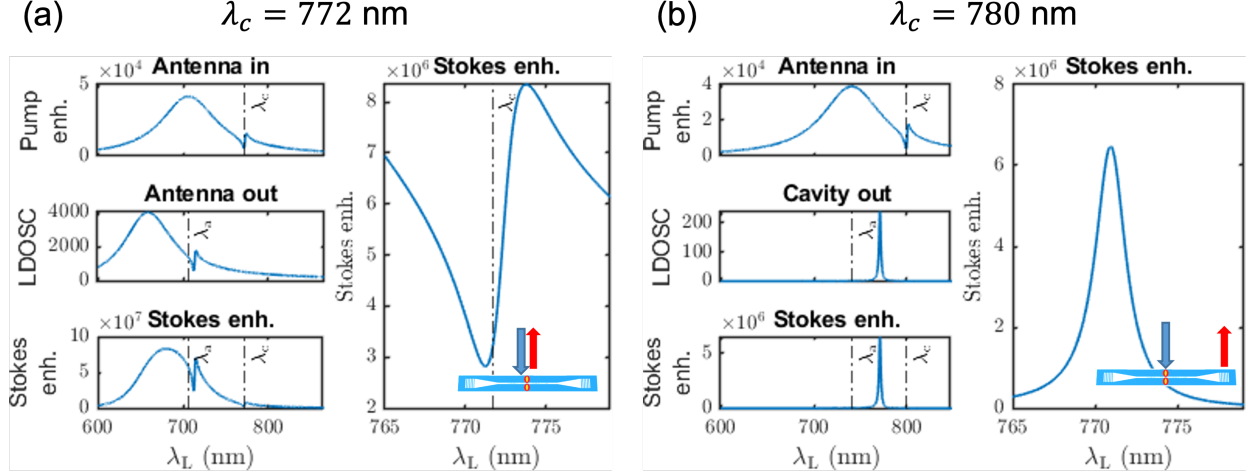


FIG. 3. Stokes enhancement vs pump wavelength obtained from a semi-analytical model. (a) corresponds to the hybrid enhancing the pump for input and output through the antenna, and (b) to the hybrid enhancing the LDOS, with an output through the cavity grating. The total Stokes enhancement (lower left panel in each case) is a product of pump enhancement (top left panel), and collected LDOS enhancement in the corresponding port (middle left panel) calculated at a frequency shifted from the laser by a the molecule's vibrational frequency. The zoomed Stokes enhancement for both hybrids (right panel) correspond to the dashed line plots of Fig. 5 (b1, c2) in the main text.

efficiencies of the antennas are estimated from the NA of the measuring objective. These are subsequently used to estimate the waveguide coupling efficiencies. For this, we compare the SERS ratio obtained for the same hybrid for identical output conditions but with an input from the grating or an input through the antenna, which depend directly on the input efficiency ratio $\eta_{\text{in}}^{\text{cav}} / \eta_{\text{in}}^{\text{ant}}$. By comparing to the theoretical model one can correctly fit this ratio with only the cavity input coupling efficiency as a free parameter (other parameters fixed from previous fit routines). Fig. 4 shows the resulting plot allowing to extract $\eta_{\text{in}}^{\text{cav}}$, and we obtain $\eta_{\text{in}}^{\text{cav}} = 0.09 \eta_{\text{in}}^{\text{ant}}$. The incoupling efficiency to the waveguide is very inefficient under the current experimental conditions, since the grating is excited with the same objective and thus a very focused spot (in the order of λ) far from the optimal plane wave case expected for gratings. The same procedure is applied to extract the output coupling efficiency and we obtain a value of $\eta_{\text{out}}^{\text{cav}} = 0.52 \eta_{\text{out}}^{\text{ant}}$, reflecting the fact that the collection of light scattered from the grating is more effective than the injection of light.

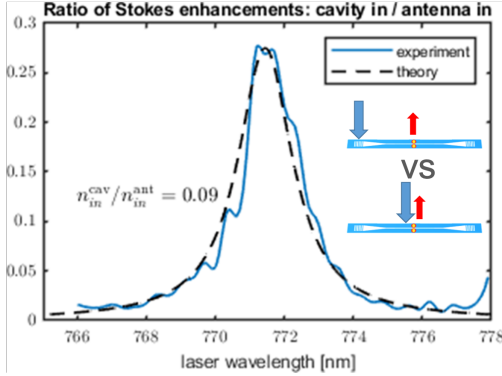


FIG. 4. Determining the input and output coupling from SERS enhancement ratios in different configurations. The input coupling efficiency is determined by fitting the ratio of SERS enhancement for same output configuration but different inputs.

Integrated SERS efficiency - In Fig. 5 the Raman spectrum enhanced by the same hybrid is shown for both free-space and integrated configuration. First observation is that integrated SERS shows no background from the silicon nitride [2], which is a unique feature of the hybrid resonator. Indeed, as opposed to simple geometries with antennas placed directly on a waveguide, here the cavity allows to filter the pump, and only the peak resonant to the hybridized cavity mode (strong peak at 473 cm^{-1}) is transmitted. Second, the good hybrid coupling allows for good emission through the cavity into the waveguide, so that an equivalent SERS enhancement is obtained for both free-space and integrated configuration. The best overall coupling is, in fact, obtained for hybrid cooperativities $4J^2/\kappa\gamma_a$ on the order of 1 [1], where $J \propto 1/\sqrt{V_c}$ is the cavity-plasmon coupling rate and κ and γ the total losses of the cavity and antenna, respectively. This is due to a trade-off between improving the exchange rate in the cavity mode when using higher Q cavities, and the lower outcoupling rate due to smaller losses [1, 3]. With the parameters obtained from the simulation, we estimate the cooperativity of these hybrids to be around $C \simeq 1.6$, ideally suited to enhance integrated operation.

LDOS dependence on cavity parameters - The total LDOS of the cavity is also directly related to the hybrid cooperativity, with a Fano contrast scaling as $C^2/(C + 1)^2$. Fig. 6 shows how the total collected LDOS depends on both the cavity quality factor and mode volume. It can be seen that the maximum LDOS is dependent only on the ratio Q_c/V_c , which is proportional to J^2/κ and thus to cooperativity. To reach higher enhancement values

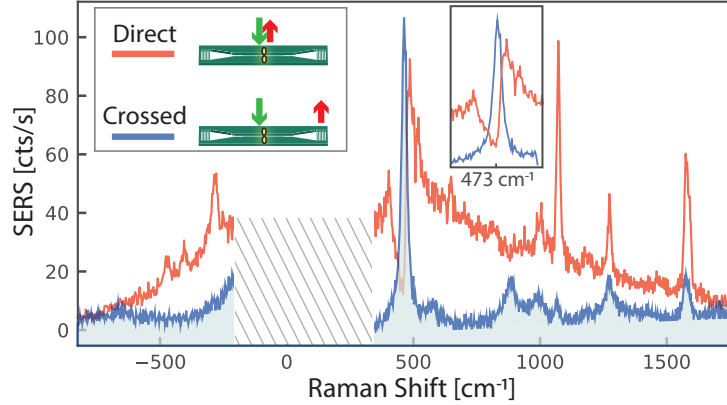


FIG. 5. Integrated SERS vs free-space. Single shot SERS for the LDOS enhancement hybrid when pumping the antenna (400 μ W pump power) and for antenna output (direct configuration) and waveguide output (crossed configuration).

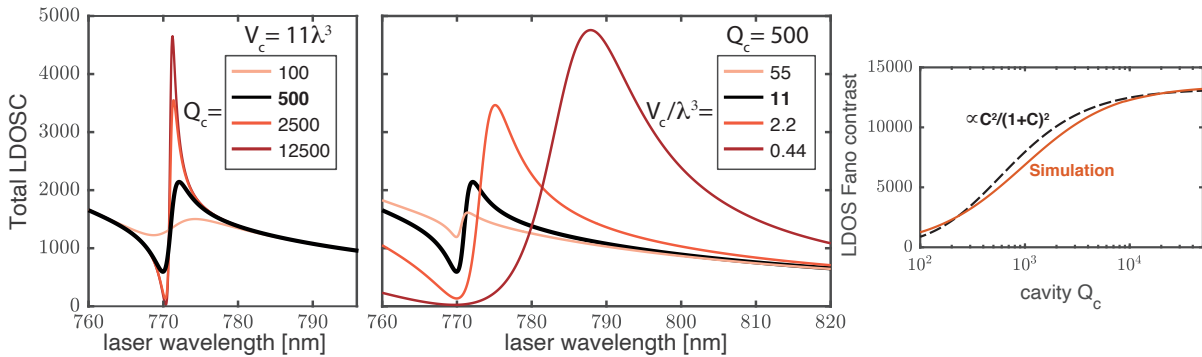


FIG. 6. Total (free-space and waveguide) collected LDOS vs cavity parameters: quality factor on the left and mode volume in the middle. The Fano contrast is mainly determined by the hybrid cooperativity, i.e. by the ratio Q_c/V_c . Right panel shows how the LDOS can be estimated by a scaling of $C^2/(C + 1)^2$ of the maximum contrast ($C \rightarrow \infty$).

while retaining small linewidths it is still preferable to increase Q_c rather than reducing V_c .

Towards coherent molecular optomechanics - The hybrid resonator enables sideband-resolved operation while maintaining good field enhancements. This paves the way towards the observation of new phenomena in SERS with few molecules, which was previously only restricted to cavity optomechanical systems. These include cooling, parametric amplification or quantum state control. Besides sideband resolution, the system needs to exhibit a good optomechanical cooperativity. For a single optical cavity mode, it

is written [4]:

$$C_m = 4 \frac{n_{\text{cav}} g_{0,m}^2}{\kappa \Gamma_m}, \quad (1)$$

with n_{cav} and κ the optical cavity's number of photons and linewidth, Γ_m the mechanical linewidth, and $g_{0,m}$ the optomechanical coupling rate. The latter can be expressed for SERS systems as a function of the Raman activity and the mode volume of the optical mode [5, 6]. Here we estimate the optomechanical cooperativity by considering the hybridized cavity mode as the only optical resonance, with modified linewidth and mode volume $\kappa_H = \kappa_c + 2J^2 \text{Im}(\chi_a(\omega_c))$ and $V_H = V_c / (2|1 + J\chi_a \sqrt{V_c/V_a}|^2)$, with V_a the antenna mode volume at the molecule's position and χ_a the antenna susceptibility [1, 3]. Using these values, we estimate the optomechanical cooperativity in our system to be $C_m \simeq 10^{-3}$. We have considered a laser power of 1 mW (deciding on the cavity photon number, here of 92 photons, and restricted to values below damage threshold as observed experimentally), for 1000 molecules (increasing by \sqrt{N} the optomechanical coupling [7]), Raman activity of $500 \text{\AA}^4/\text{amu}^{-1}$ [5] and typical optomechanical quality factor $Q_m = 200$ [8].

Although the cooperativity with this particular system is still too low to observe nonlinear effects, by only increasing Q_c to 5000 and with a realistic gap of 4 nm for the dimer, we expect $C_m \simeq 1.6$, large enough to allow for coherent optomechanical interaction and quantum control. These constraints could be further relaxed by using pulsed excitation [9].

* Equal contribution

† f.koenderink@amolf.nl

- [1] I. Shlesinger, K. G. Cognée, E. Verhagen, and A. F. Koenderink, Integrated molecular optomechanics with hybrid dielectric–metallic resonators, *ACS Photonics* **8**, 3506 (2021), <https://doi.org/10.1021/acsphotonics.1c00808>.
- [2] F. Peyskens, P. Wuytens, A. Raza, P. V. Dorpe, and R. Baets, Waveguide excitation and collection of surface-enhanced raman scattering from a single plasmonic antenna, *Nanophotonics* **7**, 1299 (2018).
- [3] H. M. Doeleman, E. Verhagen, and A. F. Koenderink, Antenna-Cavity Hybrids: Matching Polar Opposites for Purcell Enhancements at Any Linewidth, *ACS Photonics* **3**, 1943 (2016).
- [4] W. P. Bowen, G. J. Milburn, and G. J. Milburn, Quantum Optomechanics (CRC Press, 2015).

- [5] P. Roelli, C. Galland, N. Piro, and T. J. Kippenberg, Molecular cavity optomechanics as a theory of plasmon-enhanced Raman scattering, *Nat. Nanotechnol.* **11**, 164 (2016).
- [6] M. K. Schmidt, R. Esteban, A. González-Tudela, G. Giedke, and J. Aizpurua, Quantum Mechanical Description of Raman Scattering from Molecules in Plasmonic Cavities, *ACS Nano* **10**, 6291 (2016).
- [7] Y. Zhang, J. Aizpurua, and R. Esteban, Optomechanical Collective Effects in Surface-Enhanced Raman Scattering from Many Molecules, *ACS Photonics* , acsphotonics.0c00032 (2020), tex.ids= zhang_2020a.
- [8] E. C. Le Ru and P. G. Etchegoin, Chapter 4 - sers enhancement factors and related topics, in Principles of Surface-Enhanced Raman Spectroscopy, edited by E. C. Le Ru and P. G. Etchegoin (Elsevier, Amsterdam, 2009) pp. 185–264.
- [9] A. Lombardi, M. K. Schmidt, L. Weller, W. M. Deacon, F. Benz, B. de Nijs, J. Aizpurua, and J. J. Baumberg, Pulsed Molecular Optomechanics in Plasmonic Nanocavities: From Nonlinear Vibrational Instabilities to Bond-Breaking, *Physical Review X* **8**, 011016 (2018).